Archives of Civil and Mechanical Engineering (2023) 23:184
https://doi.org/10.1007/s43452-023-00722-7

ORIGINAL ARTICLE

Microstructure evolution and strain hardening behavior of thermomechanically processed low-C high-manganese steels: an effect of deformation temperature

Aleksandra Kozłowska[1] · Piotr Stawarczyk[2] · Adam Grajcar[1] · Krzysztof Radwański[2] · Krzysztof Matus[3] · Ludovic Samek[4]

Received: 23 February 2023 / Revised: 14 June 2023 / Accepted: 15 June 2023 / Published online: 30 June 2023

Abstract
Effects of reduced (– 40 °C), ambient (20 °C), and elevated (200 °C) deformation temperatures on the microstructure evolution and strain hardening behavior of two low-C thermomechanically processed high-manganese steels were studied. The microstructure was characterized by means of scanning electron microscopy (SEM), electron backscatter diffraction (EBSD), and transmission electron microscopy (TEM) techniques. The temperature-dependent tendency of austenite to strain-induced ε/α′-martensitic transformation and mechanical twinning was qualitatively and quantitatively assessed using the EBSD technique. The steel containing 26 wt% of Mn showed the beneficial strength–ductility balance at reduced deformation temperature -40 °C due to the intense Transformation-Induced Plasticity (TRIP) effect which resulted in the formation of significant ε- and α′-martensite fractions during tensile deformation. The mechanical properties of steel containing 27 wt% of Mn were more beneficial at elevated deformation temperature 200 °C due to the occurrence of intense Twinning-Induced Plasticity (TWIP) effect expressed by the presence of significant fraction of mechanical twins. Moreover, at the highest deformation temperature 200 °C, the evidence of thermally activated processes affecting the mechanical behavior of the higher Mn steel was identified and described.

Keywords High-manganese steel · Deformation temperature · Steel sheet · Twinning-induced plasticity · Transformation-induced plasticity · ε/α′-Martensite

1 Introduction

Twinning-induced plasticity (TWIP) and Transformation-induced plasticity (TRIP) high-manganese steels are characterized by high strain hardening potential, large uniform and total elongations, and high ultimate tensile strength [1]. These unique properties make these materials potentially useful for lightweight constructions in the automotive industry [2]. The beneficial mechanical properties of high-manganese steels (excellent strength–ductility combination) are related to the TWIP or TRIP effects, which occur besides dislocation slip during plastic deformation [3]. The

✉ Aleksandra Kozłowska
aleksandra.kozlowska@polsl.pl

Piotr Stawarczyk
piotr.stawarczyk@imz.pl

Adam Grajcar
adam.grajcar@polsl.pl

Krzysztof Radwański
krzysztof.radwanski@imz.pl

Krzysztof Matus
krzysztof.matus@polsl.pl

Ludovic Samek
ludovic.samek@fh-wels.at

[1] Department of Engineering Materials and Biomaterials, Faculty of Mechanical Engineering, Silesian University of Technology, Konarskiego 18a St, 44-100 Gliwice, Poland

[2] Łukasiewicz Research Network – Upper Silesian Institute of Technology, 12-14 K. Miarki Street, 44-100 Gliwice, Poland

[3] Materials Research Laboratory, Faculty of Mechanical Engineering, Silesian University of Technology, Konarskiego 18a St., 44-100 Gliwice, Poland

[4] Faculty for Engineering and Environmental Sciences, University of Applied Sciences Upper Austria, 23 Stelzhamerstrasse, 4600 Wels, Austria

deformation twins act as obstacles for dislocation movement, leading to a decrease in a dislocation glide distance [4]. This evidence, called the dynamic Hall–Petch effect, results in an increase of strain hardening rate, and as a consequence, it allows to obtain high tensile strength levels and substantial uniform and total elongations [5]. The high-Mn steels show excellent mechanical properties; the product of ultimate tensile strength and total elongation may exceed 60,000 MPa% [1]. The martensitic transformation occurring during deformation also provides the high work hardening rate and mechanical properties due to the presence of ε- or α'-martensite plates [6]. The deformation mode of high-Mn steels is strongly related to the stacking fault energy (SFE) [7]. The dominant deformation mechanism changes from martensite formation (TRIP effect) for low SFE values to mechanical twinning (TWIP effect) for higher SFE values [8].

The data available in the literature are focused mainly on the microstructure–property relationships of the high-Mn steels with increased C contents [9]. Besides the outstanding mechanical properties of high-Mn steels with the increased carbon contents (0.4–0.8 wt%), the industrial application of such steels is rather limited. The increased C content deteriorates weldability of these steels [10], which significantly reduces their use for automotive components. Moreover, high-Mn steels with the increased C content are prone to dynamic strain aging (DSA) effect, leading to reduced formability of steel sheets [11]. Therefore, the low-C high-Mn steel is the perspective material in automotive industry. In order to use the full potential of such steels, their strain hardening behavior and mechanical properties at reduced and elevated temperatures should be investigated. Jabłońska [12] reported that the heat generated during plastic deformation of TWIP steels had higher values than for conventional steels. The thermal effect of plastic deformation affects the microstructure and mechanical properties of high-Mn steels. Most of the previous research has been focused on the room temperature behavior of high-Mn steels [8]. The studies concerning the influence of reduced and elevated temperature on the intensity of TRIP/TWIP effects are still limited [13]. Most available studies concern the qualitative analysis of the microstructure evolution during deformation at different temperatures [14]. The quantitative analysis is typically provided using the XRD method [15]. However, it cannot provide the information on microstructural details.

The temperature factor occurs during forming of steel sheets and arises from adiabatic heating during dynamic deformation [16]. The most advantageous TRIP or TWIP effects should take place at a temperature corresponding to the conditions of steel processing and exploitation [17]. Therefore, the chemical composition of the steel should provide the desired strain hardening in a wide temperature range. Hence, the aim of this study was to characterize the influence of deformation temperature in a range of – 40 to 200 °C on the microstructure and mechanical properties of two low-C high-manganese steels characterized by different chemical compositions. The EBSD method providing both qualitative and quantitative analyses of the microstructure was applied in the current study. The microstructural results were analyzed together with the strain hardening behavior of investigated steels at different deformation temperatures (negative, room, and elevated). The tendency of the investigated steels to induce TRIP/TWIP effects was correlated to the SFE value. Understanding the relationships between temperature, the intensity of TRIP/TWIP effects and strain hardening behavior is critical for proper design and industrial application of high-Mn steel sheets.

2 Materials and experimental methods

2.1 Materials and thermomechanical processing

The materials used in the study were X6MnSiAlNbTi26-3–3 and X4MnSiAlNbTi27-4–2 type steels (Table 1). The investigated steels were prepared under the same conditions. First step included induction melting in a vacuum furnace and casting under argon atmosphere. After melting, the ingots were reheated at 1200 °C and hot forged in the temperature 1200 °C–900 °C. Then the steel was roughly rolled in 4 passes to 4.5-mm-thick plates, which were subjected in the next step to thermomechanical processing in 3 passes to sheets of 2.5 mm in thickness. The finishing rolling temperature was 850 °C.

2.2 Static tensile tests

Tensile specimens of 2.5 mm thickness and 12.5 mm width were prepared from the hot-rolled sheets and machined along the rolling direction. Tensile tests were carried out at a constant strain rate of 10^{-3} s^{-1} using an INSTRON 4505 universal testing machine equipped with the extensometer and an environmental chamber. The tensile tests were performed according to the requirements of the ASTM standard [18] at

Table 1 Chemical composition of investigated steels (wt.%)

Steel type	C	Mn	Si	Al	Nb	Ti	P	S	Fe
X6MnSiAlNbTi26-3–3	0.065	26.0	3.08	2.87	0.034	0.010	0.002	0.013	balance
X4MnSiAlNbTi27-4–2	0.040	27.5	4.18	1.96	0.033	0.010	0.004	0.017	balance

reduced (– 40 °C), ambient (20 °C), and elevated (200 °C) temperatures. Before the tensile tests, the samples were held at a given temperature for 30 min to obtain uniform temperature distribution over the entire section. The mechanical properties were determined based on the average values of three measurements per each deformation temperature.

2.3 Microstructure characterization

Two types of specimens were prepared for microstructural observations: at the initial state and after tensile tests at different temperatures. The specimens for microstructural observations carried out by means of scanning electron microscope (SEM) were mechanically ground using SiC papers (up to 2000 grit), polished with diamond suspension (up to 1 µm), and etched using 3% nital. The microstructural details at different deformation temperatures were revealed with the scanning electron microscope FEI Inspect-F operating at a voltage of 15 kV, working in a secondary electron (SE) detection mode.

The electron backscatter diffraction (EBSD) measurements were performed using the high-resolution JEOL JSM 7200F scanning electron microscope. Specimens were prepared by mechanical grinding followed by electrolytic polishing using a TenuPol-5 device working at a voltage of 50 V for 11 s. The A3 electrolyte by Struers at 21 °C was used. Kikuchi patterns were collected at an accelerating voltage of 17 kV, a working distance of 15 mm, and a step size of 10 nm; a sample tilt of 70° was used. The orientation data were postprocessed with OIM-TSL® data Analysis software v. 8.0 after applying one-step grain confidence index (CI) standardization clean-up procedure. The remained pixels with a confidence index CI < 0.1 were removed from the collected EBSD data**.** The criterion for the detection of twin boundaries was 60° misorientation about the < 111 > axis, with an angular tolerance of 5° within the austenite (FCC) matrix according to [19, 20]. Fractions of ε/α'-martensites and twin boundaries were estimated based on 10 measurements.

TEM lamellae obtained by focused ion beam (FIB) milling were observed with Titan 80–300 FEI S/TEM equipped with the high-angle annular dark-field (HAADF) and bright-field/dark-field (BF/DF) detectors operating at an accelerating voltage 300 kV. Specimens for microstructural analysis were cut from tensile samples according to Fig. 1.

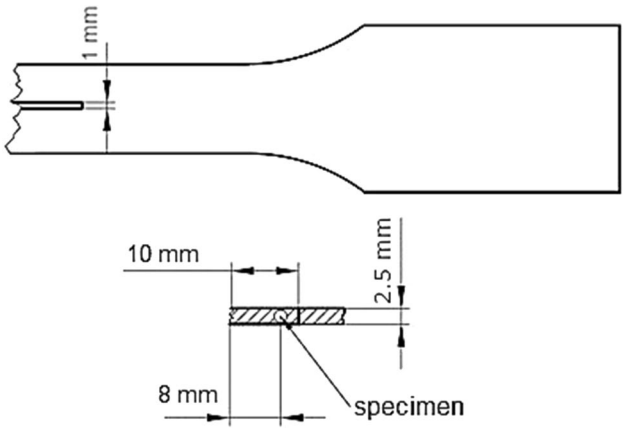

Fig. 1 Scheme showing samples' areas for SEM, EBSD, and TEM preparation

3 Results

3.1 Microstructure in the initial state

Figure 2 shows the microstructure of investigated steels in the initial state. Observed austenite grains are elongated

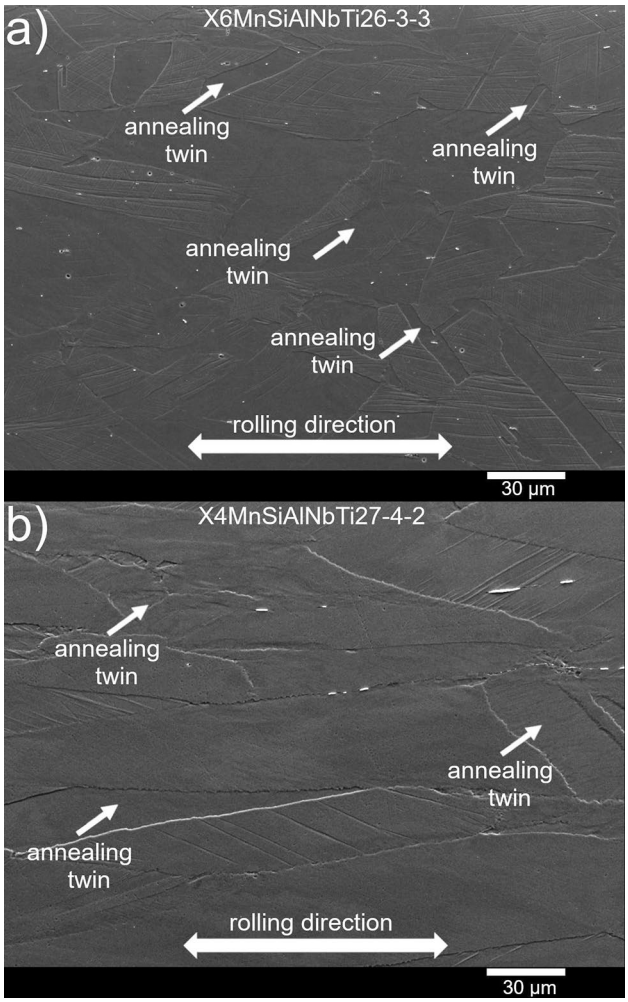

Fig. 2 SEM micrographs of the investigated steels in the initial state: X6MnSiAlNbTi26-3–3 (**a**); X4MnSiAlNbTi27-4–2 (**b**)

according to a rolling direction and numerous annealing twins were observed for both investigated steels (Fig. 2a, b). Single non-metallic inclusions were also observed. The microstructure of both steels in the initial state is fully austenitic (Fig. 3a, b). They are elongated to the rolling direction as a result of finishing rolling at a relatively low temperature of 850 °C controlled by dynamic recovery occurrence. The presence of α' or ε martensite was not detected (Fig. 3a, b).

3.2 Microstructure characterization at different deformation temperatures

Figure 4a–f shows the SEM images of the investigated steels deformed at different temperatures. The activation of twin systems in austenite grains was observed for both steels independently on a deformation temperature (some examples are marked by white arrows). Some austenite grains exhibited twinning in one preferred twin system, which may be primary twinning initiated in the low strain level. Dastur et al. [21] reported that an increase in temperature leads to an increase of twin length and thickness, which is related to an increase in the SFE. With increasing deformation temperature, the twinning intensity increased while the efficiency of strain-induced martensitic transformation decreased [14, 22, 23]. Therefore, at higher deformation temperature 200 °C, the number of active twin systems was higher (Fig. 4e, f). It was also consistent with the results obtained by other authors [19–21]. However, the detailed quantitative analysis was provided using the EBSD method. Besides deformation twins, the presence of slip lines was also observed regardless of the deformation temperature.

The temperature-dependent microstructure evolution of investigated steels was characterized using the EBSD method. The quantitative analysis was provided to estimate the intensity of the TRIP/TWIP effects at different deformation temperatures. The structural effects of tensile test carried out at -40 °C are observed in Fig. 5. The presence of ε martensite (marked as green) and a small fraction of α'-martensite (marked as red) was observed for both the investigated steels. The areas containing ε-martensite bands act as preferential sites for α'-martensite nucleation [9, 14]. The ε martensite nucleated preferentially in coarse-grained austenite grains [21]. The fraction of ε martensite was significantly higher for X6MnSiAlNbTi26-3–3 steel (Fig. 5a). Based on the literature data [1, 19], the formation of ε martensite is suppressed for the SFE higher than ca. 25 mJ m^{-2}. The SFE calculated using the JMatPro software was ~ 14 mJ m^{-2} for X6MnSiAlNbTi26-3–3 and 24 mJ m^{-2} for X4MnSiAlNbTi27-4–2 steels, respectively (Table 2).

The intensity of strain-induced martensitic transformation was higher for the steel with the lower SFE value. The fraction of twin boundaries (marked as blue in Fig. 5c, d) was similar for both investigated steels: 5% and 4% for X6MnSiAlNbTi26-3–3 and X4MnSiAlNbTi27-4–2 steels, respectively. However, the twin boundaries observed in X4MnSiAlNbTi27-4–2 were thicker and more developed. Moreover, the mechanical twinning was activated in more than one system.

Increasing the deformation temperature to 20 °C resulted in reduced fractions of ε-and α'-martensites in steel containing 26 wt% of Mn (Fig. 6a). The presence of martensite was not observed in steel with the higher Mn content (Fig. 6b). The calculated SFE was ~ 24 mJ m^{-2} for X6MnSiAlNbTi26-3–3 and 34 mJ m^{-2} for X4MnSiAlNbTi27-4–2 steels, respectively (Table 2). The SFE for the steel containing 27 wt% of Mn is within the SFE range characteristic for TWIP steels [1, 19]. The amount of twin boundaries slightly increased when compared to the specimens deformed at – 40 °C (Fig. 6c, d). Deformation twins nucleate and grow

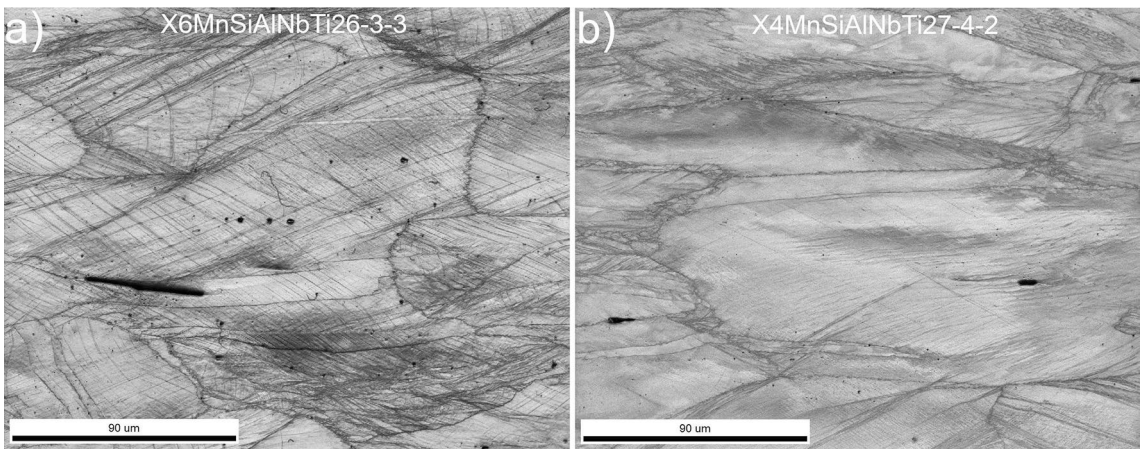

Fig. 3 EBSD maps of the investigated steels in the initial state: IQ combined with phase maps (austenite marked in gray) for X6MnSiAlNbTi26-3–3 steel (**a**) and X4MnSiAlNbTi27-4–2 steel (**b**)

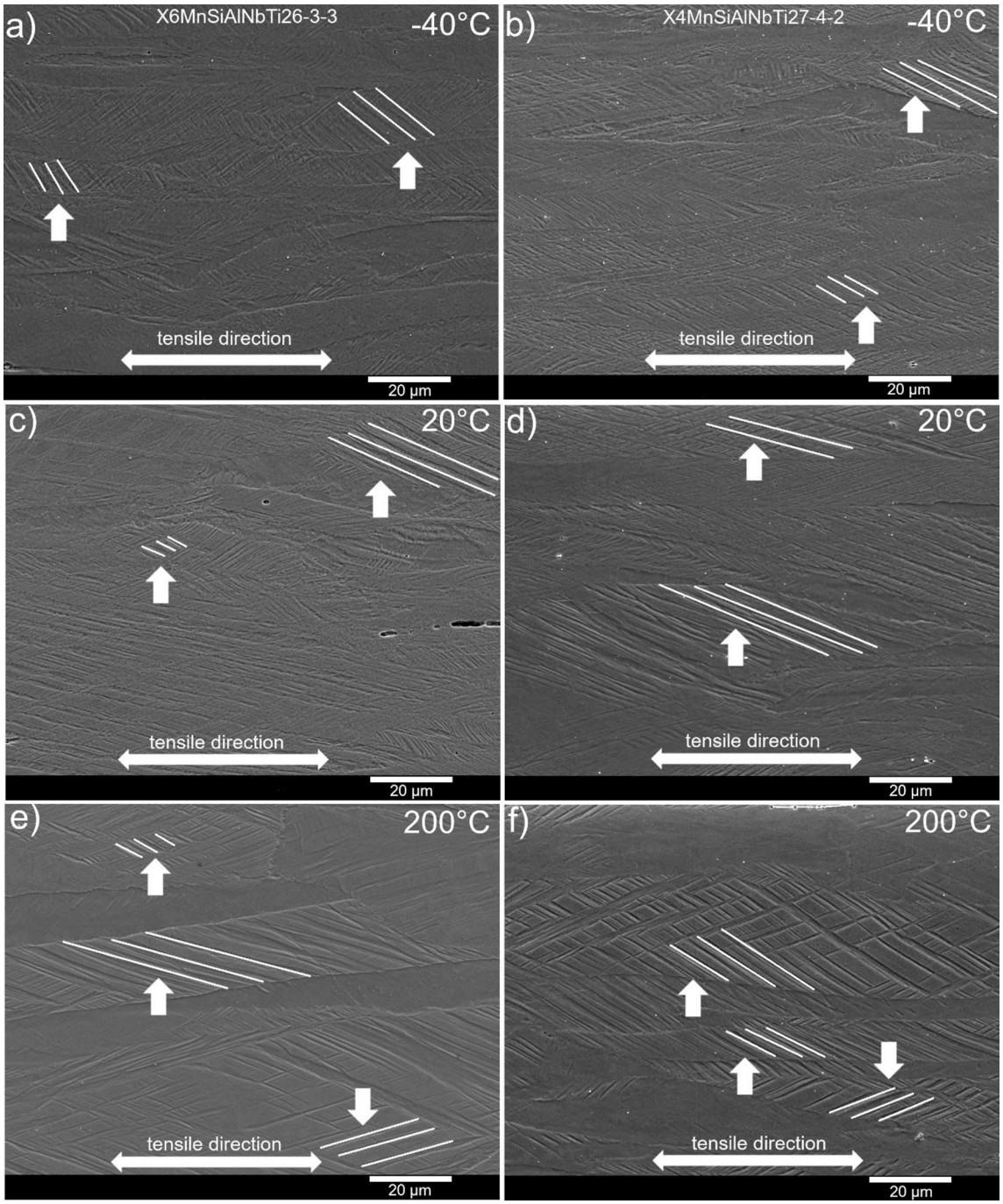

Fig. 4 SEM images of investigated steels deformed at different temperatures. X6MnSiAlNbTi26-3–3 steel deformed at – 40 °C (**a**), 20 °C (**c**), and 200 °C (**e**); X4MnSiAlNbTi27-4–2 steel deformed at – 40 °C (**b**), 20 °C (**d**), and 200 °C (**f**). Activated twins systems are marked by white arrows

mainly in coarse austenite grains because grain boundaries act as strong obstacles for their growth [13].

The calculated SFE at 200 °C rose to ~ 42 mJ m^{-2} for X6MnSiAlNbTi26-3–3 and 51 mJ m^{-2} for X4MnSiAlNbTi27-4–2 steels, respectively (Table 2). Therefore, no ε-or α′-martensites were observed in the deformed samples (Fig. 7a, b). The fractions of twin boundaries observed in both investigated steels deformed at 200 °C (Fig. 7c, d) were significantly higher than those at lower deformation temperatures. It is related to the further increase of SFE. At the highest deformation temperature, both investigated steels showed the SFE values typical for the

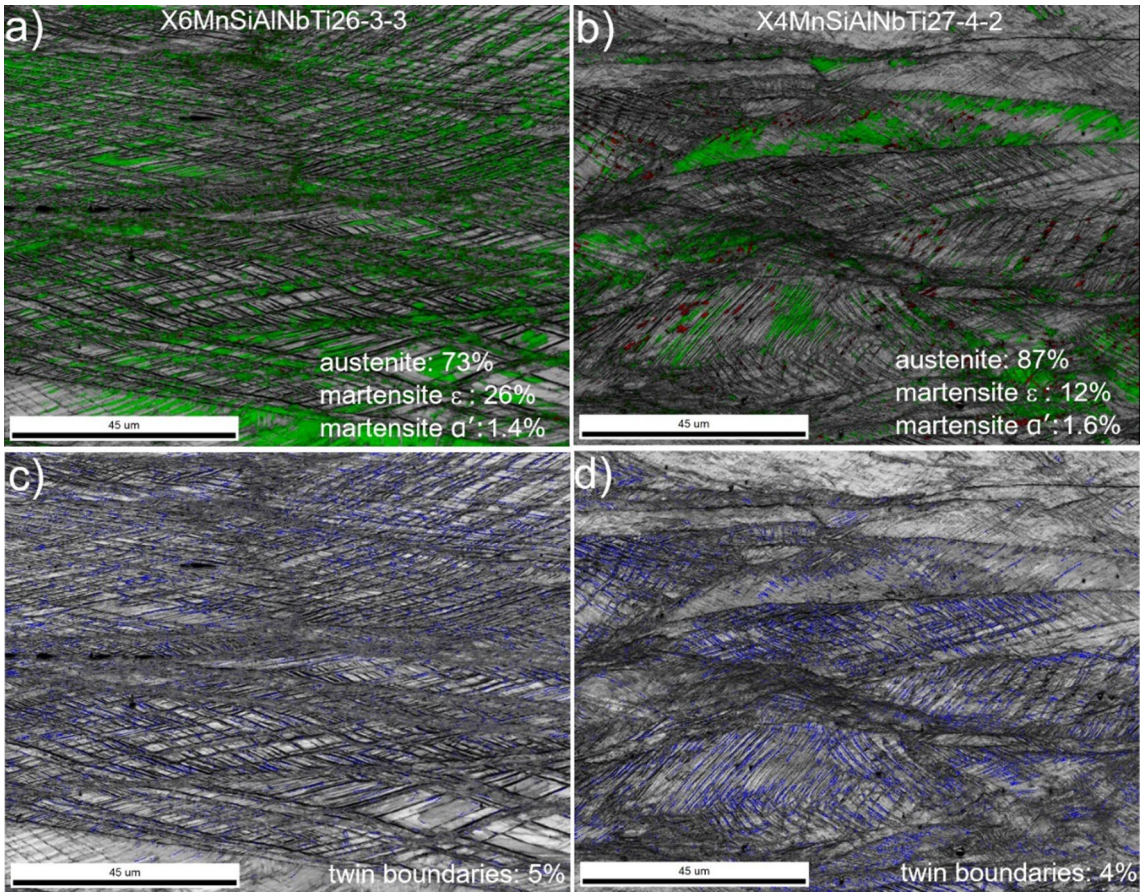

Fig. 5 EBSD maps of the investigated steels deformed at reduced temperature – 40 °C: IQ maps combined with phase maps (austenite marked in gray, martensite ε marked in green, martensite α'marked in red): X6MnSiAlNbTi26-3–3 steel (**a**), X4MnSiAlNbTi27-4–2 steel (**b**); IQ maps with twin boundaries marked in blue: X6MnSiAlNbTi26-3–3 steel (**c**), X4MnSiAlNbTi27-4–2 steel (**d**)

Table 2 Stacking fault energy (SFE) of investigated steels at different deformation temperatures calculated using JMatPro software

Steel grade	SFE, mJ m^{-2}	
	X6MnSiAlNbTi26-3–3	X4MnSiAlNbTi27-4–2
– 40 °C	14	24
20 °C	24	34
200 °C	42	51

intense TWIP effect [1, 19]. The distribution of mechanical twins in X4MnSiAlNbTi27-4–2 steel was very dense leading to small twin spacing (Fig. 7d). A high fraction of mechanical twins and small spacing between individual twins provide the increased strain hardening rate [13]. It means that the mechanical twinning was very effecive in X4MnSiAlNbTi27-4–2 steel deformed at 200 °C. The spacing between individual twin boundaries in X6MnSiAlNbTi26-3–3 steel was considerably lower; thus, the contribution of mechanical twinning to the strain hardening was smaller.

3.3 Mechanical properties and strain hardening behavior at different temperatures

The SFE controls the effectiveness of deformation mechanisms in TRIP/TWIP steels. Since, the SFE strongly depends on temperature, it has a major influence on mechanical properties of investigated steels. True stress–strain curves at different deformation temperatures obtained in static tensile tests are shown in Fig. 8a. The flow behavior of investigated steels is homogeneous without serrations in the stress–strain curves regardless of the deformation temperature.

For both investigated steels, the yield and tensile strengths decreased with increasing deformation temperature. The most beneficial strength properties were observed at – 40 °C for both the tested steels (Table 3). It was expressed by the lowest YS/UTS ratio. The YS and UTS for X6MnSiAlNbTi26-3–3 steel were 577 MPa and 834 MPa, respectively, whereas the obtained YS and UTS values for

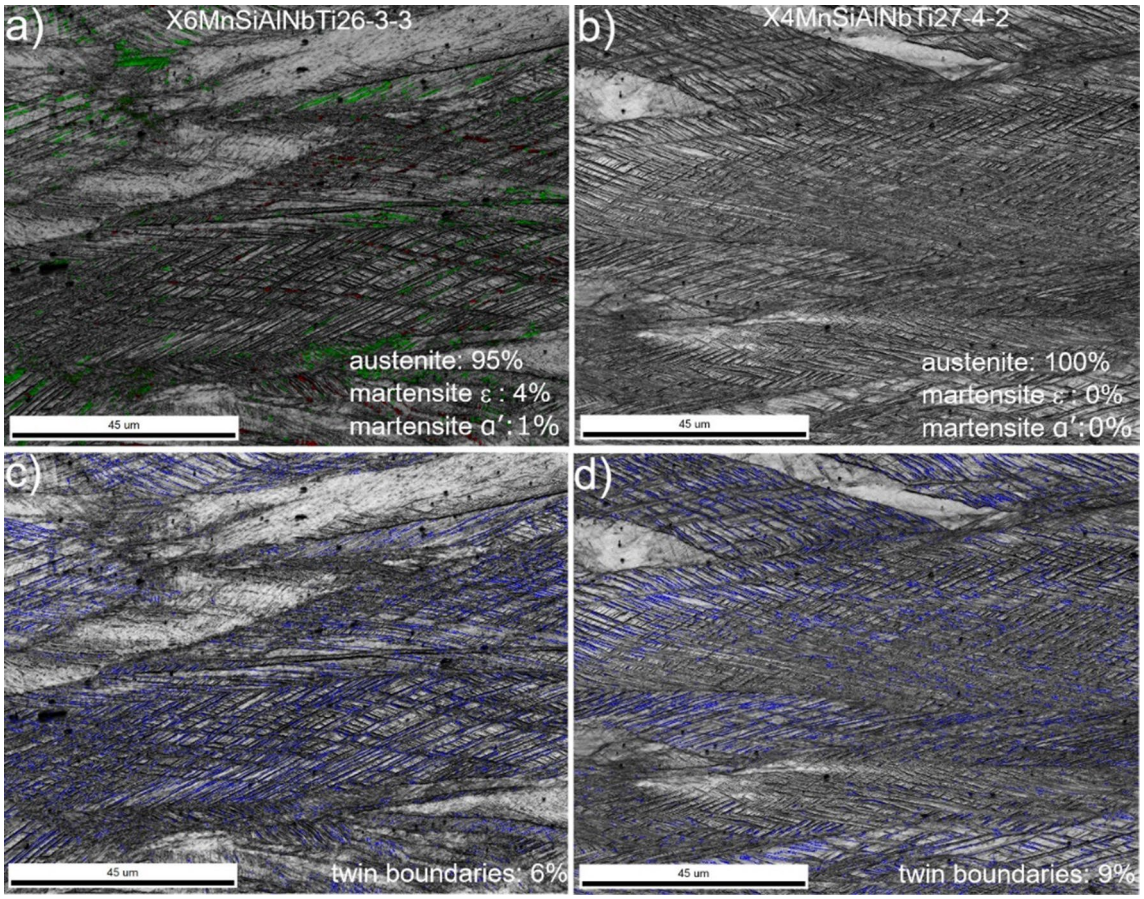

Fig. 6 EBSD maps of the investigated steels deformed at 20 °C: IQ maps combined with phase maps (austenite marked in gray, martensite ε marked in green, martensite α'marked in red): X6MnSiAlNbTi26-3–3 steel (**a**), X4MnSiAlNbTi27-4–2 steel (**b**); IQ maps with twin boundaries marked in blue: X6MnSiAlNbTi26-3–3 steel (**c**), X4MnSiAlNbTi27-4–2 steel (**d**)

X4MnSiAlNbTi27-4–2 steel were 631 MPa and 881 MPa, respectively. The lowest strength properties were noted for specimens deformed at 200 °C. The YS and UTS for X6MnSiAlNbTi26-3–3 steel were 519 MPa and 604 MPa, respectively. The obtained YS and UTS values for X4MnSiAlNbTi27-4–2 steel were 494 MPa and 615 MPa, respectively. In general, the X4MnSiAlNbTi27-4–2 steel showed higher strength properties when compared to X6MnSiAlNbTi26-3–3 steel regardless of the deformation temperature. An effect of deformation temperature on ductility of investigated steels was different. The X6MnSiAlNbTi26-3–3 steel showed higher total elongation than X4MnSiAlNbTi27-4–2 steel at reduced (– 40 °C) and ambient (20 °C) temperatures. When the temperature increased up to 200 °C, total elongation of X6MnSiAlNbTi26-3–3 steel dropped up to 22.4%, whereas X4MnSiAlNbTi27-4–2 steel showed the highest elongation: ~ 47%.

The observed strain hardening behavior of investigated steels was directly related to the intensity of TRIP/TWIP effects at particular deformation temperatures (Fig. 8b). The deformation twinning or the presence of ε- or α′-martensite plates contributes to high work hardening rate through modification of the dislocation structure [9, 14] and leads to high uniform and total elongations. At the lowest deformation temperature – 40 °C, both the steels showed the high work hardening rate (WHR) due to the formation of significant fraction of ε/α′ martensite during deformation. When the strain is above 0.05, investigated steels still showed the high WHR values when compared to the higher deformation temperature. It may be related to the formation of α′-martensite during deformation. The formation of this type of martensite requires higher strain levels [24]. The WHR decreased with increasing deformation temperature. For the specimens deformed at 20 °C and 200 °C when the strain is above 0.05, the WHR decreased rapidly and then stabilized at a similar level up to rupture. The stabilization of WHR at the strain level above 0.05 is due to the gradual formation of mechanical twins during deformation [1, 24]. The relationship among deformation temperature, the intensity of TRIP/TWIP effects, and mechanical properties of investigated steel is shown in Fig. 9.

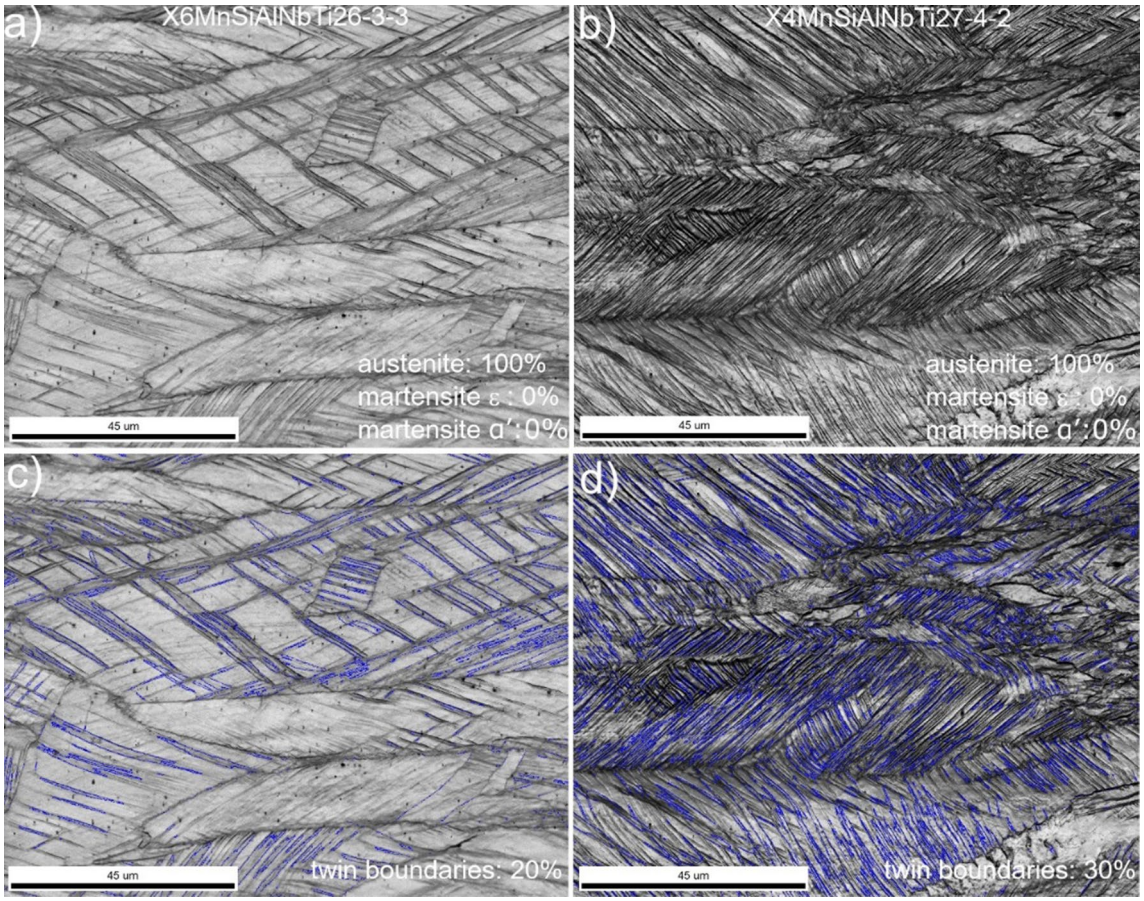

Fig. 7 EBSD maps of the investigated steels deformed at elevated temperature 200 °C: IQ maps combined with phase maps (austenite marked in gray, martensite ε marked in green, martensite α′ marked in red): X6MnSiAlNbTi26-3–3 steel (**a**), X4MnSiAlNbTi27-4–2 steel (**b**). IQ maps with twin boundaries marked in blue: X6MnSiAlNbTi26-3–3 steel (**c**), X4MnSiAlNbTi27-4–2 steel (**d**)

4 Discussion

The SFE is a key factor affecting the mechanical properties of the high-Mn steels. Besides chemical composition, the change in the temperature affects changes in the SFE, which promotes different deformation mechanisms [1, 19, 24, 25]. Generally, an increase in deformation temperature causes an increase of SFE values. TRIP effect is dominant when SFE is lower than 25 mJ/m^2—some fraction of austenite transforms into ε- or α′-martensite. When the SFE value is in a range of 25–60 mJ/m^2, deformation twins of different intensity occur (TWIP effect). If the SFE value is higher than 60 mJ/m^2, steel is strengthened mostly by dislocation glide [9, 23, 26]. The mentioned type of hardening mechanism dominant at a specific temperature range depends on the chemical composition of the steel. Zambrano [27] calculated the SFE for various high-Mn steels. He reported that an increase in the Mn content in a range of 20 to 35 wt% results in a significant increase in the SFE of austenite. An addition of Si decreases the SFE, while for Al the tendency is opposite [28]. This study is focused mainly on the differences in SFE values and resulting differences in the intensity of TRIP/TWIP effects at particular deformation temperatures rather than the effect of single alloying additives. The differences in SFE were compared with the quantitative analysis of TRIP/TWIP effects using the EBSD method. Results listed in Table 2 showed that X4MnSiAlNbTi27-4–2 steel showed the higher SFE than X6MnSiAlNbTi26-3–3 steel regardless of the deformation temperature. The SFE increased with the increase in temperature, which is similar with the trend observed by other authors for high-Mn steels [19, 24, 27, 28].

The results of the present study showed the presence of ε- and α′-martensites for both the investigated steels deformed at − 40 °C. At the reduced deformation temperature, the amount of ε-bands was high and spacing between individual ε-bands was relatively low (Fig. 5a, b). Figure 10 shows TEM bright-field and dark-field images of X6MnSiAlNbTi26-3–3 steel deformed at − 40 °C and selected area electron diffraction (SAED) patterns corresponding to the ε-martensite.

The detailed EBSD measurements show that α′-martensite plates nucleated at the intersections of ε-martensite bands;

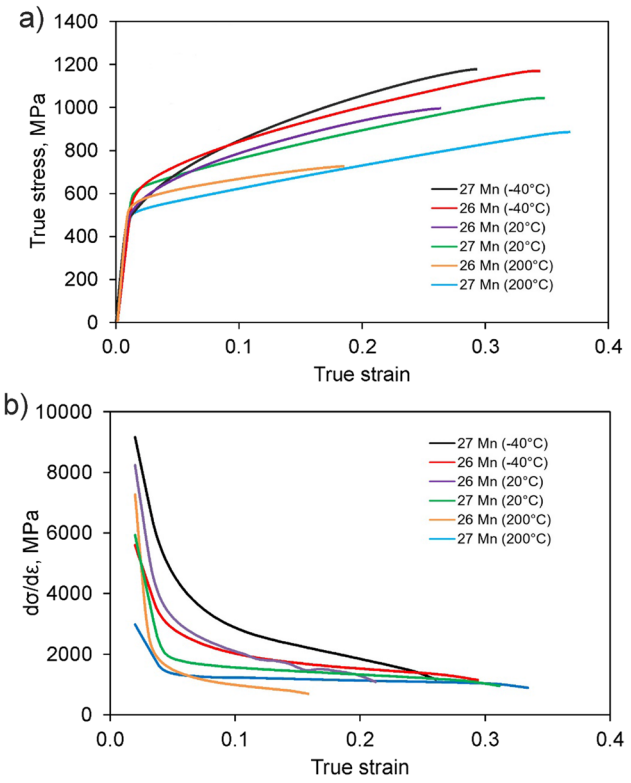

Fig. 8 Mechanical behavior of investigated steels at different temperatures in the uniform deformation range: true stress–true strain curves (**a**); work hardening rate as a function of true strain (**b**)

however, more frequently they were formed along the ε-martensite bands (Fig. 11a). Martensite α′ occurred in the darkest areas characterized by low values of the IQ parameter (Fig. 11b). The ε-martensite was observed in the areas characterized by significantly higher IQ parameter. It means that the dislocation density in α′ is very high and the formation of such type of martensite requires a higher strain level.

The presence of α′-martensite was also confirmed using TEM technique. Figure 12 shows the TEM bright-field and dark-field images of X6MnSiAlNbTi26-3–3 steel deformed at – 40 °C and SAED patterns corresponding to the α′-martensite. The α′-martensite plates of various thicknesses from about 0.1 µm to 0.6 µm were formed in the austenite matrix. The α′-martensite plates were located in the areas of high dislocation density. The presence of stacking faults (SF) located near α′-martensite was also observed (Fig. 12a). Olson et al. [29, 30] reported that the α′-martensite may nucleate on bundles or SF packets.

The results of the present study and data reported by other authors [15, 22] show that austenite in TRIP-aided high-Mn steels transforms into α′-martensite according to the sequence: γ (fcc) → ε (hcp) → α' (bcc). The gradual nucleation of ε- and α′-martensites during plastic deformation leads to the formation of strong barriers for dislocation motion, which increases the strain hardening rate. The number of slip systems is the least in the ε-martensite due to the close packed hexagonal structure [31]. Li et al. [31] reported that formation of strain-induced ε-martensite is not favorable for the toughness of high-Mn TRIP steel. The planar void sheets along {111}γ are easy to form at intersections of ε-martensite plates during impact deformation. However, strain-induced α′-martensite transformation enhances the toughness at RT because α′-martensite impedes transgranular relative to intergranular fracture.

More intense TRIP effect accompanied with the formation of mechanical twins was observed in X6MnSiAlNbTi26-3–3 at -40 °C (Fig. 5), which allowed to obtain high mechanical properties (Fig. 8, Table 3). An increase in the deformation temperature to 20 °C resulted in little reduction of strength properties of both investigated steels, while the plasticity was at a similar level (Fig. 8, Table 3). The reduction of strength properties was more pronounced in X4MnSiAlNbTi27-4–2 steel. The significant decrease in the amount of ε- and α′-martensites was observed in X6MnSiAlNbTi26-3–3 steel deformed at 20 °C (Fig. 6a), while this type of constituents was not observed in X4MnSiAlNbTi27-4–2 steel (Fig. 6b). Increasing the deformation temperature to 200 °C resulted in the suppression of ε- and α′-martensite formation in both the investigated steels. It is related to the further increase in SFE (Table 2). The significant decrease in total elongation was noted for X6MnSiAlNbTi26-3–3 steel deformed at 200 °C (TEl = 22.4%). The opposite trend was noted for X4MnSiAlNbTi27-4–2 steel (TEl = 47.2%). It is due to the higher efficiency of TWIP effect and higher density of deformation twins (Fig. 7c, d). The most intense mechanical twinning in steel containing 26 wt% of Mn is shifted to the higher deformation temperatures. It is related to the lower SFE of this steel caused by the lower Mn and higher Si contents. The increased plasticity of steel containing 27% of Mn at 200 °C is also related to the occurrence of thermally activated processes accompanied

Table 3 Mechanical properties of investigated steels at different deformation temperatures

Steel grade	UTS, MPa		YS, MPa		TEl, %		YS/UTS	
	26 Mn	27 Mn	26 Mn	27 Mn	26 Mn	27Mn	26Mn	27Mn
-40 °C	834 ± 21	881 ± 26	577 ± 28	631 ± 23	43.4 ± 3.2	35.1 ± 2.8	0.69	0.72
20 °C	743 ± 18	767 ± 20	554 ± 10	561 ± 21	43.8 ± 2.9	33.5 ± 2.4	0.75	0.73
200 °C	604 ± 11	615 ± 15	509 ± 16	494 ± 13	22.4 ± 1.7	47.2 ± 2.4	0.84	0.80

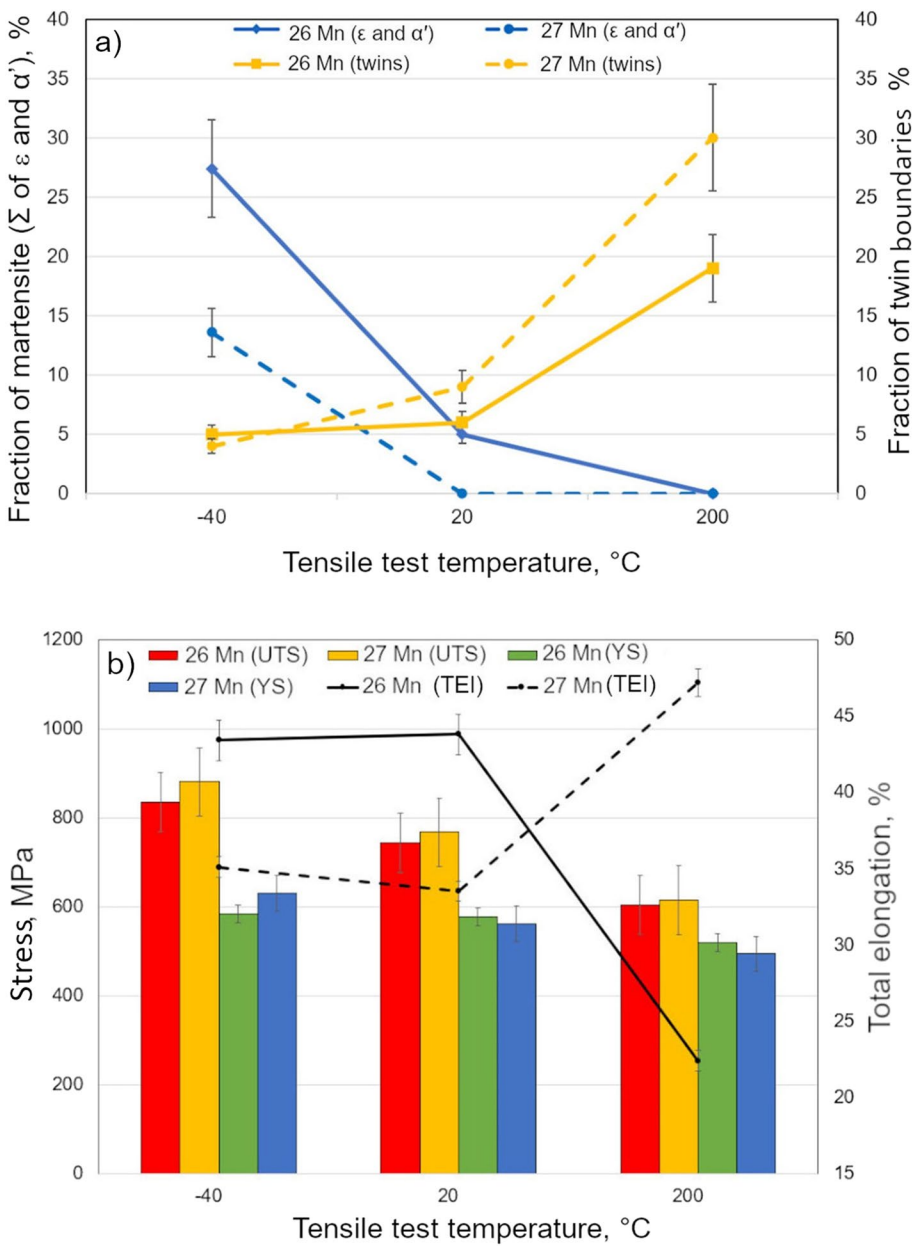

Fig. 9 Mechanical properties at different temperatures and accompanying microstructural changes: fraction of ε/α′-martensites and twin boundaries (**a**); summarized tensile test results (**b**)

with subgrains and dislocation cells formation (Fig. 13). It means that during tensile deformation, the early stage of dynamic recovery took place. Such effect was not observed in X6MnSiAlNbTi26-3–3 steel deformed at 200 °C. It may be related to the higher strength properties of X4MnSiAlNbTi27-4–2 steel resulted in a higher internal friction [32] occurring during tensile deformation.

5 Conclusions

In the present study, an effect of deformation temperature on the microstructure evolution and mechanical properties of X6MnSiAlNbTi26-3–3 and X4MnSiAlNbTi27-4–2 steels of different Mn, Si, and Al contents was analyzed. The temperature-dependent tendency of the investigated steels to ε/α′-martensite formation and mechanical twinning was correlated with the work hardening behavior. The important findings of the current study were as follows:

- The X6MnSiAlNbTi26-3–3 steel of lower SFE showed the highest mechanical properties at reduced deformation temperature – 40 °C. It was due to the intense TRIP effect which resulted in the formation of significant fractions of ε- and α′-martensites during tensile deformation. The YS, UTS, and TEl were 577 MPa, 834 MPa, and 43.4%, respectively.

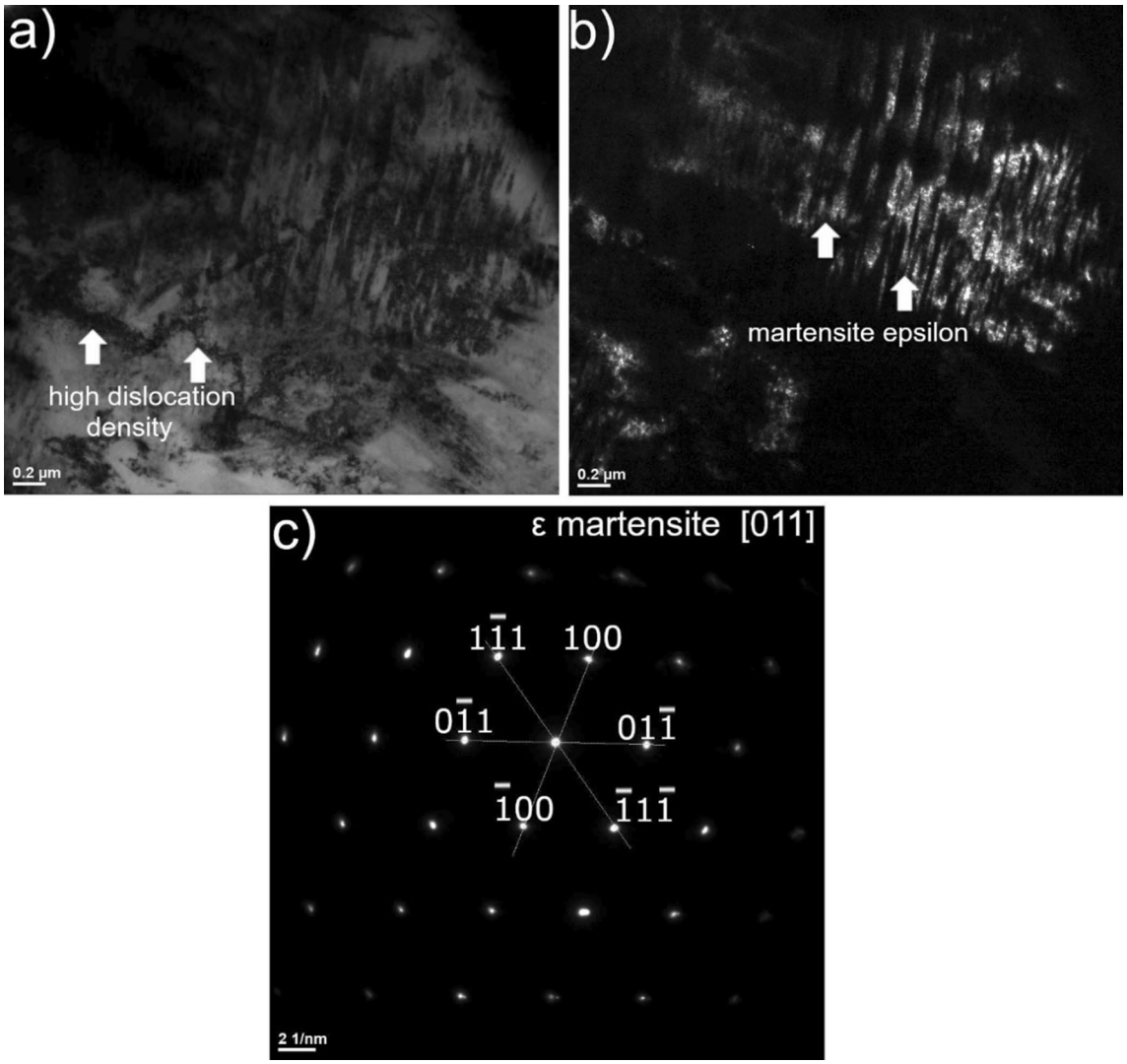

Fig. 10 TEM micrographs of X6MnSiAlNbTi26-3–3 steel deformed at – 40 °C: bright field (**a**); dark field of ε-martensite (**b**); SAED pattern of ε-martensite (**c**)

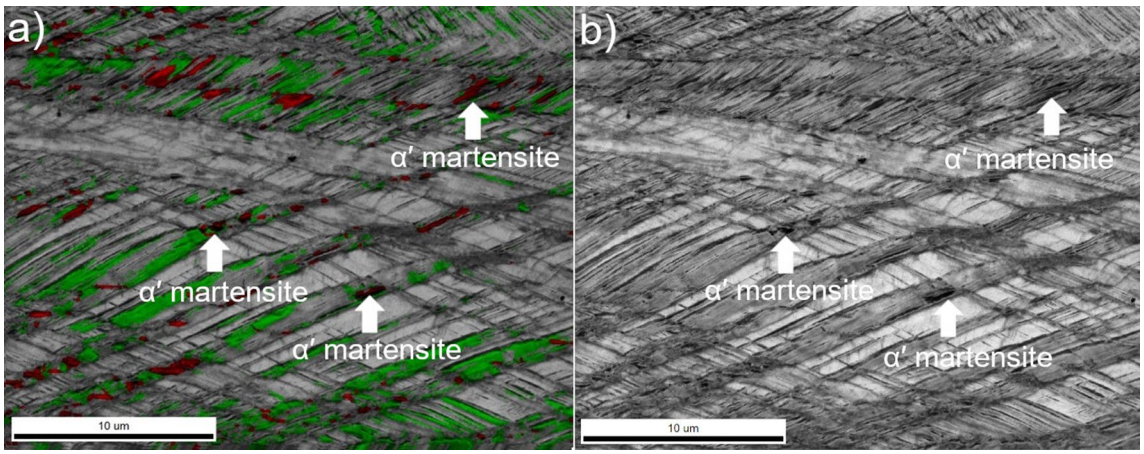

Fig. 11 EBSD images for X6MnSiAlNbTi26-3–3 steel deformed at -40 °C: IQ maps combined with phase maps (austenite marked in gray, martensite ε marked in green, martensite α'marked in red) (**a**); IQ map (**b**)

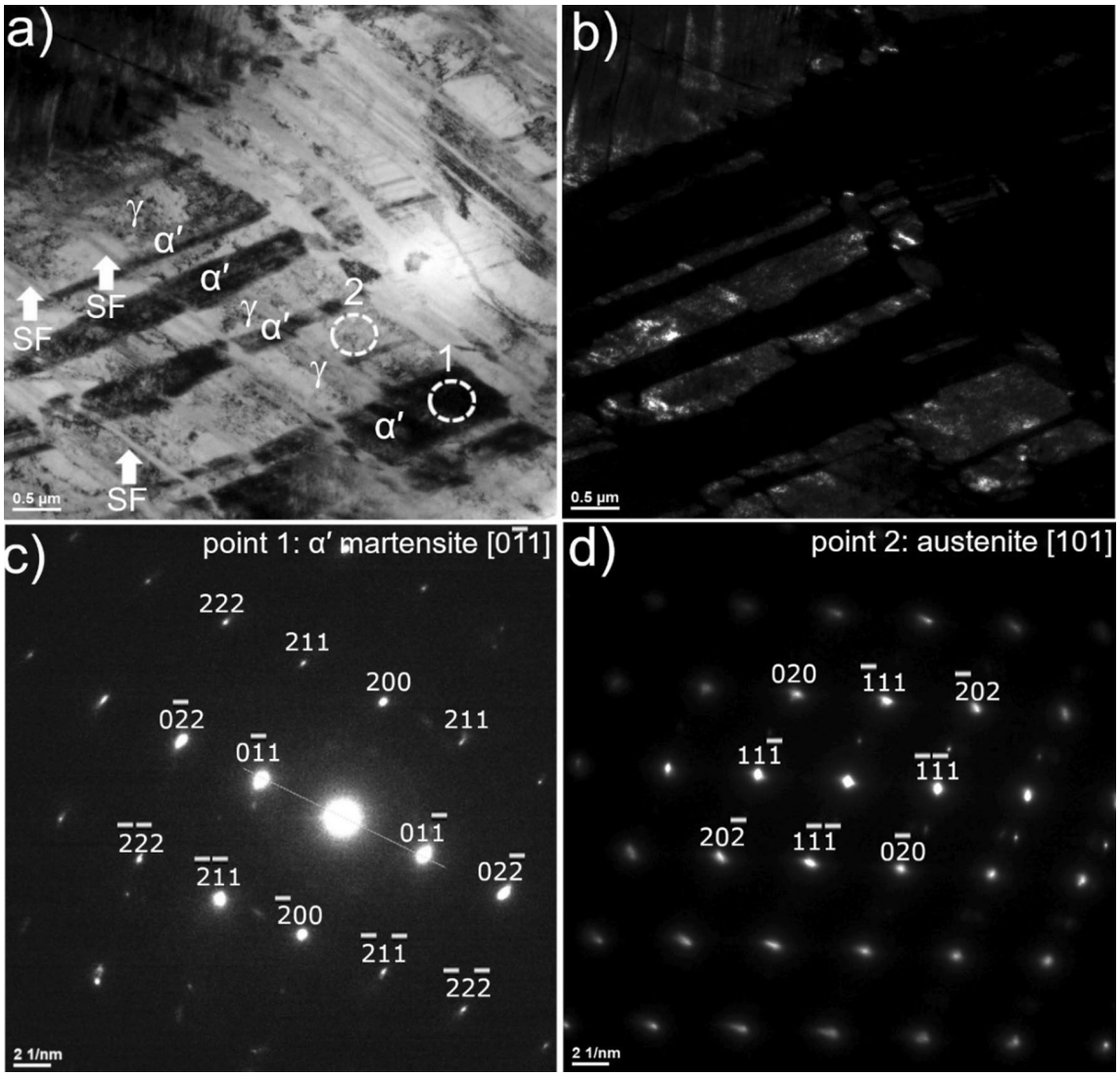

Fig. 12 TEM micrographs of X6MnSiAlNbTi26-3–3 steel deformed at − 40 °C: bright field (**a**); dark field of α′-martensite (**b**); SAED pattern of α′-martensite corresponding to the area marked as point 1 (**c**); SAED pattern of austenite corresponding to the area marked as point 2

- The mechanical properties of X4MnSiAlNbTi27-4–2 steel of higher SFE were more beneficial at elevated deformation temperature 200 °C due to the occurrence of intense TWIP effect expressed by the presence of significant fraction of mechanical twins in the microstructure. The YS, UTS, and TEl were 494 MPa, 615 MPa, and 47.2%, respectively.
- Besides intense mechanical twinning, the increased plasticity of X4MnSiAlNbTi27-4–2 steel at 200 °C was also caused by the dynamic recovery accompanied with the formation of subgrains and dislocation cells.
- A high fraction of mechanical twins and its very dense distribution provided to the increased strain hardening rate of X4MnSiAlNbTi27-4–2 at elevated deformation temperature 200 °C, while the high amount of ε-bands and low spacing between individual ε-bands contributed to the increased strain hardening rate of X6MnSiAlNbTi26-3–3 steel at reduced deformation temperature – 40 °C.

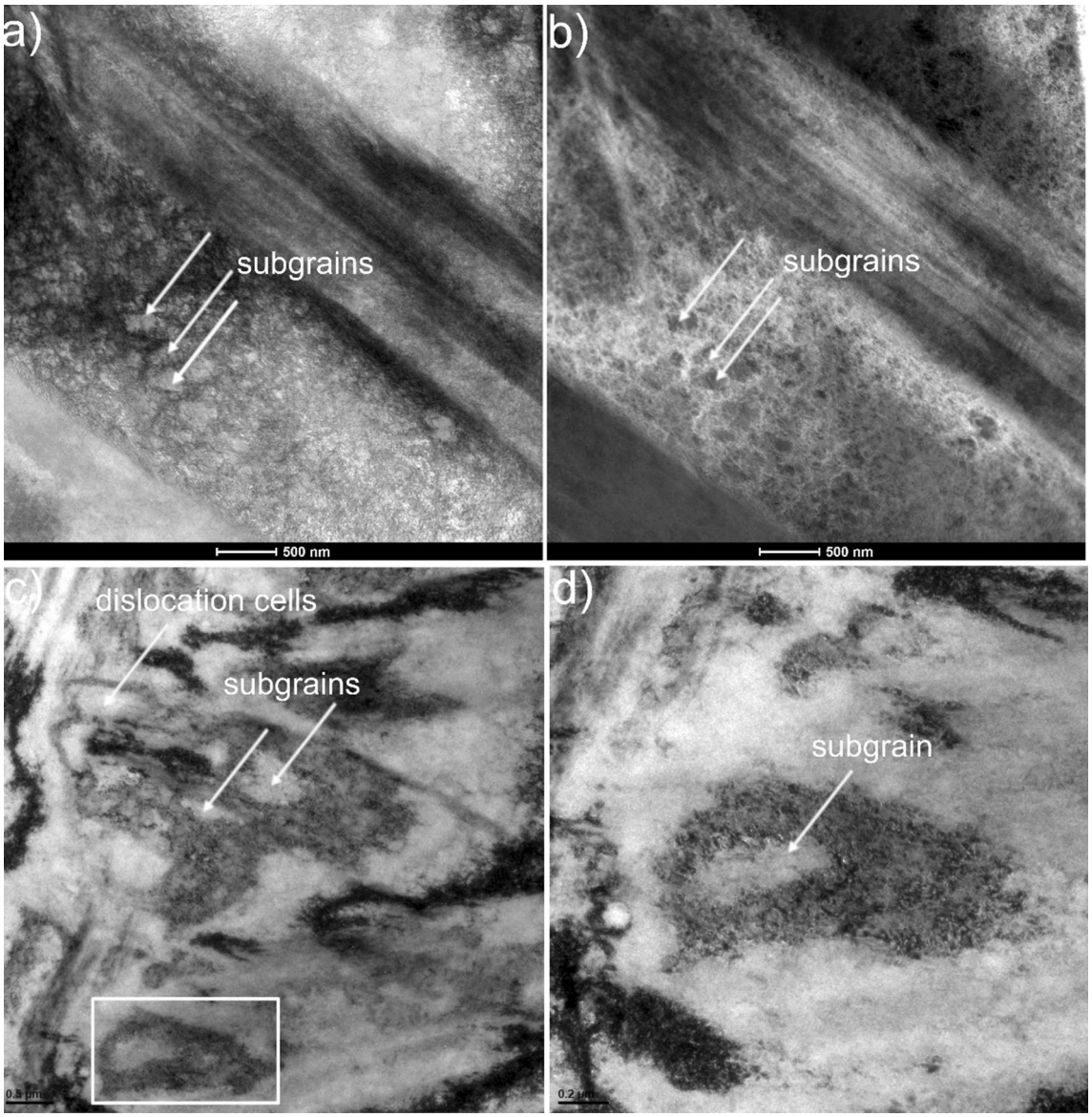

Fig. 13 STEM and TEM micrographs of X4MnSiAlNbTi27-4–2 steel deformed at 200 °C: bright-field STEM with diffraction contrast (**a**); HAADF STEM with chemical contrast (**b**); bright-field TEM (**c**); magnification of the area marked by white rectangle (**d**)

Acknowledgements This research was supported by a rector grant in the area of scientific research and development works, Silesian University of Technology (grant no. 10/010/RGJ21/1031).

Funding The financial support of the National Science Center, Poland, is gratefully acknowledged, Grant No. 2017/27/B/ST8/02864.

Data availability statement The data that support the findings of this study are available from the corresponding author upon reasonable request.

Declarations

Conflict of interest The authors declare that they have no conflict of interest.

Ethical approval The authors state that the research was conducted according to ethical standards.

References

1. De Cooman BC, Estrin Y, Kim SK. Twinning-induced plasticity (TWIP) steels. Acta Mater. 2018;142:283–362. https://doi.org/10.1016/j.actamat.2017.06.046.
2. Jabłońska MB, Kowalczyk K. Microstructural aspects of energy absorption of high manganese steels. Procedia Manuf. 2019;27:91–7. https://doi.org/10.1016/j.promfg.2018.12.049.
3. Grajcar A, Kciuk M, Topolska S, Płachcińska A. Microstructure and corrosion behaviour of hot-deformed and cold-strained high-Mn steels. J Mater Eng Perform. 2016;25:2245–54. https://doi.org/10.1007/s11665-016-2085-5.
4. Galindo-Nava EI, Rivera-Diaz-del-Castillo PEJ. Understanding martensite and twin formation in austenitic steels: A model describing TRIP and TWIP effects. Acta Mater. 2017;128:120–34. https://doi.org/10.1016/j.actamat.2017.02.004.
5. Śmiglewicz A, Jabłońska M, Moćko W, Kowalczyk K, Hadasik E. Properties and structure of X30MnAlSi26-4-3 high strength steel subjected to dynamic compression processes. Arch Metall Mater. 2017;62:2255–60. https://doi.org/10.1515/amm-2017-0332.
6. Grajcar A, Opiela M, Fojt-Dymara G. The influence of hot-working conditions on a structure of high-manganese steel. Arch Civ Mech Eng. 2009;9:49–58. https://doi.org/10.1016/S1644-9665(12)60217-9.
7. Pierce DT, Benzing JT, Jiménez JA, Hickel T, Bleskov I, Keumf, J. et al. The influence of temperature on the strain-hardening behavior of Fe-22/25/28Mn-3Al-3Si TRIP/TWIP steels. Materialia. 2022;22:101425, doi:https://doi.org/10.1016/j.mtla.2022.101425.
8. Pierce DT, Jimenez JA, Bentley J, Raabe D, Oskay C, Wittig J. The influence of manganese content on the stacking fault and austenite/ε-martensite interfacial energies in Fe–Mn–(Al–Si) steels investigated by experiment and theory. Acta Mater. 2014;68:238–53. https://doi.org/10.1016/j.actamat.2014.01.001.
9. Allain S, Bouaziz O, Chateau J. Thermally activated dislocation dynamics in austenitic FeMnC steels at low homologous temperature. Scripta Mater. 2010;62:500–5003. https://doi.org/10.1016/j.scriptamat.2009.12.026.
10. Yang J, Dong H, Xia Y, Li P, Wu W, Wang B. Precipitation behavior of carbides and cryogenic toughness in heat-affected zone of high-Mn twinning-induced plasticity steel welded joint. J Manuf Process. 2021;68:716–27. https://doi.org/10.1016/j.jmapro.2021.06.003.
11. Kozłowska A, Grzegorczyk B, Morawiec M, Grajcar A. Explanation of the PLC effect in advanced high-strength medium-Mn steels. A review Materials. 2019;12:4175. https://doi.org/10.3390/ma12244175.
12. Jabłońska MB. Effect of the conversion of the plastic deformation work to heat on the behaviour of TWIP steels: a review. Arch Civ Mech Eng. 2023;23:135. https://doi.org/10.1007/s43452-023-00656-0.
13. Chen J, Li S, Ren JK, Liu ZY. Temperature dependence of deformation behaviors in high manganese austenitic steel for cryogenic applications. Materials. 2021;14:5426. https://doi.org/10.3390/ma14185426.
14. Shterner V, Timokhina IB, Beladi H. On the work-hardening behaviour of a high manganese TWIP steel at different deformation temperatures. Mater Sci Eng A. 2016;669:437–46. https://doi.org/10.1016/j.msea.2016.05.104.
15. Kowalska J, Ryś J, Cios G, Bednarczyk W. The effect of reduced temperatures on microstructure development in tensile tested high-manganese steel. Mater. Sci. Eng. A. 2019;767:138406, doi :https://doi.org/10.1016/j.msea.2019.138406.
16. Jabłońska MB, Jasiak K, Kowalczyk K, Bednarczyk I, Skwarski M, Tkocz M, Gronostajski Z. Deformation behaviour of high-manganese steel with addition of niobium under quasi-static tensile loading. Mater Sci Poland. 2022;40:1–11. https://doi.org/10.2478/msp-2022-0029.
17. Finfrock C, Bhattacharya S, McBrady B, Ballard T, Clarke AM, Clarke K. Decoupling the impacts of strain rate and temperature on TRIP in a Q&P steel. JOM. 2022;74:506–12. https://doi.org/10.1007/s11837-021-05039-5.
18. ASTM E8/E8M-13a. Standard test methods for tension testing of metallic materials. West Conshohocken: ASTM International, 2013.
19. Mosecker L, Pierce DT, Schwedt A, Beighmohamadi M, Mayer J, Bleck W, et al. Temperature effect on deformation mechanisms and mechanical properties of a high manganese C+N alloyed austenitic stainless steel. Mater Sci Eng A. 2015;642:71–83. https://doi.org/10.1016/j.msea.2015.06.047.
20. Saeed-Akbari A, Mosecker L, Schwedt A, Bleck W. Characterization and prediction of flow behavior in high-manganese Twinning Induced Plasticity steels: Part I. Mechanism maps and work-hardening behavior. Metall. Mater. Trans. A. 2012;43:1688–1704, doi:https://doi.org/10.1007/s11661-011-0993-4.
21. Dastur Y, Leslie W. Mechanism of work hardening in Hadfield manganese steel. Metall Mater Trans A. 1981;12:749–59. https://doi.org/10.1007/BF02648339.
22. Curtze S, Kuokkala VT. Dependence of tensile deformation behavior of TWIP steels on stacking fault energy, temperature and strain rate. Acta Mater. 2010;58:5129–41. https://doi.org/10.1016/j.actamat.2010.05.049.
23. Ren J, Mao D, Gao Y, Chen J, Liu Z. High carbon alloyed design of a hot-rolled high-Mn austenitic steel with excellent mechanical properties for cryogenic application. Mater. Sci. Eng. A. 2021;827:141959, doi:https://doi.org/10.1016/j.msea.2021.141959.
24. Xiong R, Peng H, Wang S, Haitao S, Wen Y. Effect of stacking fault energy on work hardening behaviors in Fe–Mn–Si–C high manganese steels by varying silicon and carbon contents. Mater Des. 2015;85:707–14. https://doi.org/10.1016/j.matdes.2015.07.072.
25. Bouaziz O, Zurob H, Chehab B, Embury JD, Allain S, Huang M. Effect of chemical composition on work hardening of Fe—Mn—C TWIP steels. Mater Sci Technol. 2021;27:707–9. https://doi.org/10.1179/026708309X12535382371852.
26. Timokhina IB, Medvedev A, Lapovok R. Severe plastic deformation of a TWIP steel. Mater Sci Eng A. 2014;593:163–9. https://doi.org/10.1016/j.msea.2013.11.013.
27. Zambrano OA. Stacking fault energy maps of Fe–Mn–Al–C–Si steels: Effect of temperature, grain size, and variations in compositions. J Eng Mater Technol. 2016;138:1021–5. https://doi.org/10.1115/1.4033632.
28. Chen L, Zhao Y, Qin X. Some Aspects of high manganese Twinning-Induced Plasticity (TWIP) steel, A review. Acta Metall. Sin. (Engl. Lett.). 2013;26:1–15, doi: https://doi.org/10.1007/s40195-012-0501-x.
29. Olson GB, Cohen M. A mechanism for the strain-induced nucleation of martensitic transformations. J Less Common Met. 1972;28:107–18.
30. Olson GB, Cohen M. A general mechanism of martensitic nucleation: Part II. fcc→bcc and other martensitic transformations. Metall. Trans. A. 1976;7:1905–1914.
31. Li X, Chen L, Zhao Y, Misra RDK. Influence of manganese content on ε-/α′-martensitic transformation and tensile properties of low-C high-Mn TRIP steels. Mater Des. 2018;142:190–202. https://doi.org/10.1016/j.matdes.2018.01.026.

32. Steinmetz DR, Japel T, Wietbrock B, Eisenlohr P, Gutierrez-Urrutia I, Saeed-Akbari A, Hickel T, Roters F, Raabe D. Revealing the strain-hardening behavior of twinning-induced plasticity steels: Theory, simulations, experiments. Acta Mater. 2013;61:494–510. https://doi.org/10.1016/j.actamat.2012.09.064.